Kirchhoff prestack depth migration in velocity models with and without vertical gradients: Comparison of triclinic anisotropy with simpler anisotropies

Václav Bucha
Department of Geophysics, Faculty of Mathematics and Physics, Charles University in Prague, Ke Karlovu 3, 121 16 Praha 2, Czech Republic,
E-mail: bucha@seis.karlov.mff.cuni.cz

Summary

The Kirchhoff prestack depth migration is used to calculate migrated sections in simple heterogeneous and homogeneous anisotropic velocity models in order to demonstrate the impact of anisotropy and simple inhomogeneity on migrated images. We generate the recorded wave field in velocity models composed of two layers separated by a non-inclined curved interface. The anisotropy of the upper layer is triclinic and the layer has a constant vertical gradient of elastic moduli. The bottom layer is isotropic and homogeneous. We apply the Kirchhoff prestack depth migration to both heterogeneous and homogeneous single-layer velocity models with different types of anisotropy: a triclinic anisotropic medium, transversely isotropic media with a horizontal symmetry axis and a vertical symmetry axis. We show and discuss the errors of the migrated interface caused by inaccurate velocity models used for migration. The study is limited to P-waves.

Keywords

3-D Kirchhoff prestack depth migration, anisotropic velocity model, velocity gradient

1. Introduction

We continue in the Kirchhoff prestack depth migration studies performed by Bucha (2011, 2012a, 2012b). The dimensions of the velocity model, shot-receiver configuration, methods of calculating the recorded wave field and the migration are the same as in the papers by Bucha (2011, 2012a, 2012b). Our aim is to study the influence of the incorrect anisotropy and incorrect heterogeneity on the migrated image.

We generate the synthetic data using the ray theory. To calculate the synthetic recorded wave field, we use two simple anisotropic velocity models composed of two layers separated by one curved interface which is non-inclined in the direction perpendicular to the source-receiver profiles. For computing the recorded wave field, Bucha (2011, 2012a) used a homogeneous upper layer with triclinic anisotropy. Bucha (2012b) used an inhomogeneous upper layer with triclinic anisotropy and with vertical or horizontal constant gradients of elastic moduli. In this paper we use two different constant vertical gradients of elastic moduli, both greater than the gradient used by Bucha (2012b). The bottom layer is homogeneous and isotropic.

We migrate the synthetic data using the 3-D ray-based Kirchhoff prestack depth migration. Distortions of the imaged curved interface induced by incorrect anisotropy

In: Seismic Waves in Complex 3-D Structures, Report 23 (Department of Geophysics, Charles University, Prague, 2013), pp. 45–59

and incorrect heterogeneity are evaluated using several anisotropic migration velocity models. The models consist of a single layer without the interface. In the first two heterogeneous velocity models, the distribution of elastic moduli corresponds to the upper layer of the velocity models in which the synthetic data have been calculated. Additional six incorrect velocity models are homogeneous and their anisotropy is either triclinic, or transversely isotropic with a horizontal symmetry axis or a vertical symmetry axis.

We show mispositioning, distortion and defocusing of the migrated interface caused by inaccurate velocity models used for migration. We use 3-D migration because the reflected two-point rays propagate in triclinic media in a 3-D volume. The study is limited to P-waves.

2. Anisotropic velocity models with a vertical velocity gradient

The dimensions of the velocity models and measurement configurations are derived from the 2-D Marmousi model and dataset (Versteeg & Grau, 1991). The horizontal dimensions of the velocity model are 9.2 km x 10 km ($x_1 \times x_2$ coordinate axes) and the depth is 3 km (x_3 axis). The velocity model is composed of two layers separated by one non-inclined curved interface (see Figure 1).

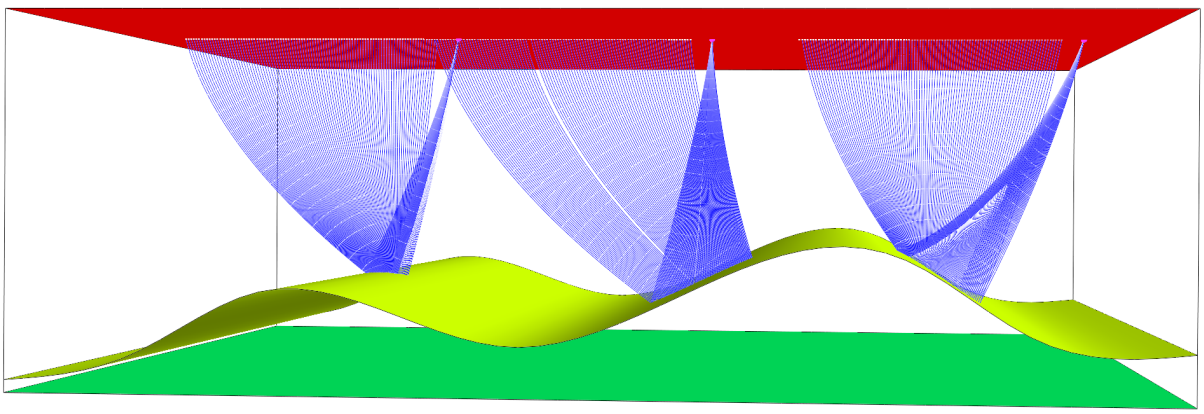

Figure 1. Velocity model with a non-inclined curved interface. The horizontal dimensions of the velocity model are 9.2 km x 10 km ($x_1 \times x_2$ axes), the depth is 3 km (x_3 axis). Velocity model contains one curved interface which is non-inclined in the direction perpendicular to the source-receiver profiles. Two-point rays of the reflected P-wave for one selected profile line and three shot-receiver configurations (at horizontal coordinate $x_2 = 4$ km) are calculated in the velocity model with triclinic anisotropy and a vertical velocity gradient (TA-VG2 medium).

2.1. Velocity models for the recorded wave field

The recorded wave field is computed in two velocity models composed of two layers with the triclinic anisotropy representing dry Vosges sandstone (Mensch & Rasolofosaon, 1997). Each model has a different velocity gradient in the upper layer. The bottom layer is isotropic and homogeneous. The medium in the upper layer is triclinic and is specified by two matrices of density-reduced elastic moduli A_{ij} in km^2/s^2.

The first model has a TA-VG1 medium and the matrix of density-reduced elastic moduli at the depth of $x_3 = 0$ km (values specified by Mensch & Rasolofosaon (1997) are multiplied by constant 0.4) reads

$$\begin{pmatrix} 4.12 & 0.36 & 0.52 & 0.56 & 0.44 & 0.32 \\ & 4.24 & 0.84 & 0.08 & -0.08 & -0.24 \\ & & 5.64 & 0.00 & -0.20 & -0.40 \\ & & & 2.04 & 0.00 & 0.08 \\ & & & & 2.40 & 0.00 \\ & & & & & 1.96 \end{pmatrix} . \tag{1}$$

The second model has a TA-VG2 medium and the matrix of density-reduced elastic moduli at the depth of $x_3 = 0$ km (values specified by Mensch & Rasolofosaon (1997) are multiplied by constant 0.1) reads

$$\begin{pmatrix} 1.03 & 0.09 & 0.13 & 0.14 & 0.11 & 0.08 \\ & 1.06 & 0.21 & 0.02 & -0.02 & -0.06 \\ & & 1.41 & 0.00 & -0.05 & -0.10 \\ & & & 0.51 & 0.00 & 0.02 \\ & & & & 0.60 & 0.00 \\ & & & & & 0.49 \end{pmatrix} . \tag{2}$$

The matrix for both models at the depth of $x_3 = 2.9$ km (values specified by Mensch & Rasolofosaon (1997)) reads

$$\begin{pmatrix} 10.3 & 0.9 & 1.3 & 1.4 & 1.1 & 0.8 \\ & 10.6 & 2.1 & 0.2 & -0.2 & -0.6 \\ & & 14.1 & 0.0 & -0.5 & -1.0 \\ & & & 5.1 & 0.0 & 0.2 \\ & & & & 6.0 & 0.0 \\ & & & & & 4.9 \end{pmatrix} . \tag{3}$$

The density-reduced elastic moduli inside the layer are determined by linear interpolation from the specified values of density-reduced elastic moduli. The bottom layer is isotropic and the P-wave velocity in the layer is $V_p = 3.6$ km/s.

2.2. Velocity models for the migration

The migration is performed using correct single-layer (without an interface) heterogeneous velocity models with triclinic anisotropy and vertical velocity gradients (reference media TA-VG1 and TA-VG2 specified in Section 2.1).

In addition, we migrate in incorrect single-layer *homogeneous* velocity models with the triclinic anisotropy (TA-VG1M, TA-VG2M media), VTI symmetry (VTI-1-VG1M, VTI-1-VG2M media) and HTI symmetry (HTI-2-VG1M, HTI-2-VG2M media).

Constant elastic moduli A^0_{ij} for homogeneous velocity models with the TA-VG1M and TA-VG2M media are calculated from the correct heterogeneous velocity models (TA-VG1 and TA-VG2 media) using equation:

$$A^0_{ij} = \left[\frac{\sqrt{A_{ij}(x_3)} + \sqrt{A_{ij}(0)}}{2} \right]^2 , \tag{4}$$

where

- $A_{ij}(x_3)$ are elastic moduli determined by linear interpolation at the depth x_3, in this paper we use the arithmetic mean of the depth of the interface $x_3 = 2.4125$ km,
- $A_{ij}(0)$ are elastic moduli at the depth of $x_3 = 0$ km.

For derivation, see Appendix A.

2.2.1. Homogeneous velocity models with triclinic anisotropy

TA-VG1M is the triclinic anisotropic medium and the matrix of elastic moduli reads

$$\begin{pmatrix} 6.43 & 0.56 & 0.81 & 0.87 & 0.69 & 0.50 \\ & 6.62 & 1.31 & 0.12 & -0.12 & -0.37 \\ & & 8.81 & 0.00 & -0.31 & -0.62 \\ & & & 3.19 & 0.00 & 0.12 \\ & & & & 3.75 & 0.00 \\ & & & & & 3.06 \end{pmatrix}. \tag{5}$$

TA-VG2M is the triclinic anisotropic medium and the matrix of elastic moduli reads

$$\begin{pmatrix} 3.94 & 0.34 & 0.50 & 0.54 & 0.42 & 0.31 \\ & 4.06 & 0.80 & 0.08 & -0.08 & -0.23 \\ & & 5.40 & 0.00 & -0.19 & -0.38 \\ & & & 1.95 & 0.00 & 0.08 \\ & & & & 2.30 & 0.00 \\ & & & & & 1.88 \end{pmatrix}. \tag{6}$$

2.2.2. Homogeneous velocity models with a transversely isotropic medium with a vertical symmetry axis

VTI-1-VG1M is a transversely isotropic medium with a vertical symmetry axis. The matrix of elastic moduli reads

$$\begin{pmatrix} 6.53 & 0.41 & 1.06 & 0.00 & 0.00 & 0.00 \\ & 6.53 & 1.06 & 0.00 & 0.00 & 0.00 \\ & & 8.81 & 0.00 & 0.00 & 0.00 \\ & & & 3.47 & 0.00 & 0.00 \\ & & & & 3.47 & 0.00 \\ & & & & & 3.06 \end{pmatrix}. \tag{7}$$

VTI-1-VG2M is a transversely isotropic medium with a vertical symmetry axis. The matrix of elastic moduli reads

$$\begin{pmatrix} 4.00 & 0.25 & 0.65 & 0.00 & 0.00 & 0.00 \\ & 4.00 & 0.65 & 0.00 & 0.00 & 0.00 \\ & & 5.40 & 0.00 & 0.00 & 0.00 \\ & & & 2.12 & 0.00 & 0.00 \\ & & & & 2.12 & 0.00 \\ & & & & & 1.88 \end{pmatrix}. \tag{8}$$

We fitted matrix elements A_{33} for vertical P-waves and elements $A_{13} = A_{23}$ (mean of triclinic elements A_{13}, A_{23}) for near vertical P-waves according to the elastic moduli of homogeneous models with triclinic anisotropy (matrices (5) and (6)). Horizontal P-wave velocities (elements A_{11}, A_{22}) are equal in both directions and the value is the mean of triclinic elements A_{11}, A_{22}.

2.2.3. Homogeneous velocity models with a transversely isotropic medium with a horizontal symmetry axis

HTI-2-VG1M is a transversely isotropic medium with a horizontal symmetry axis. The symmetry axis is parallel with the x_2 coordinate axis. The matrix of elastic moduli reads

$$\begin{pmatrix} 8.81 & 1.31 & 1.31 & 0.00 & 0.00 & 0.00 \\ & 6.62 & 1.31 & 0.00 & 0.00 & 0.00 \\ & & 8.81 & 0.00 & 0.00 & 0.00 \\ & & & 3.19 & 0.00 & 0.00 \\ & & & & 3.75 & 0.00 \\ & & & & & 3.19 \end{pmatrix}. \tag{9}$$

HTI-2-VG2M is a transversely isotropic medium with a horizontal symmetry axis. The symmetry axis is parallel with the x_2 coordinate axis. The matrix of elastic moduli reads

$$\begin{pmatrix} 5.40 & 0.80 & 0.80 & 0.00 & 0.00 & 0.00 \\ & 4.06 & 0.80 & 0.00 & 0.00 & 0.00 \\ & & 5.40 & 0.00 & 0.00 & 0.00 \\ & & & 1.95 & 0.00 & 0.00 \\ & & & & 2.30 & 0.00 \\ & & & & & 1.95 \end{pmatrix}. \tag{10}$$

We fitted matrix elements A_{33} for vertical P-waves and elements A_{13} for near vertical P-waves according to the elastic moduli of homogeneous models with triclinic anisotropy (matrices (5) and (6)). The horizontal P-wave velocity, parallel with the profile lines (elements A_{11}), is equal to the vertical P-wave velocity (elements A_{33}) of the homogeneous models with triclinic anisotropy.

3. Shots and receivers

The measurement configuration is derived from the Marmousi model and dataset (Versteeg & Grau, 1991). The profile lines are parallel with the x_1 coordinate axis. Each profile line has the following configuration: The first shot is 3 km from the left-hand side of the velocity model, the last shot is 8.975 km from the left-hand side of the velocity model, the distance between the shots is 0.025 km, and the depth of the shots is 0 km. The total number of shots along one profile line is 240. The number of receivers per shot is 96, the first receiver is located 2.575 km left of the shot location, the last receiver is 0.2 km left of the shot location, the distance between the receivers is 0.025 km, and the depth of the receivers is 0 km. This configuration simulates a simplified towed streamed acquisition geometry.

The 3-D measurement configuration consists of 81 parallel profile lines, see Figure 2. The distance between the parallel profile lines is 0.025 km.

4. Recorded wave field

The recorded wave field in the triclinic velocity models with vertical velocity gradients were computed using the ANRAY software package (Gajewski & Pšenčík, 1990). 3-D ray tracing is used to calculate the two-point rays of the reflected P-wave. We then compute the ray-theory seismograms at the receivers. The two-point rays do not stay in the vertical planes corresponding to the individual profiles.

In the velocity model with the non-inclined curved interface, the recorded wave field is equal for all parallel profile lines, because the distribution of elastic moduli is 1-D and the non-inclined curved interface is independent of the coordinate x_2 perpendicular to the profile lines (2.5-D velocity model, see Figures 1, 2).

We calculate the recorded wave field in two heterogeneous velocity models with triclinic anisotropy and two different vertical gradients in the upper layer. As specified in Section 2.1, the gradients are defined by matrices (1), (2) and (3) of density-reduced elastic moduli A_{ij} at two different depths of $x_3 = 0$ and 2.9 km.

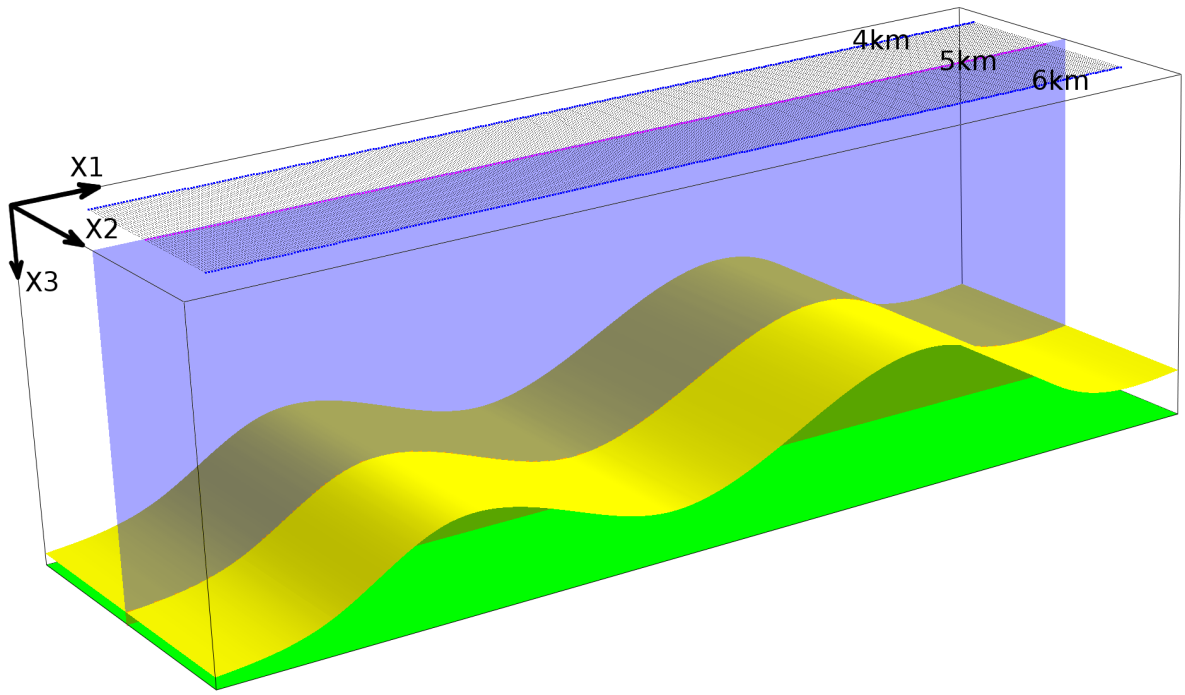

Figure 2. Part of the velocity model with 81 parallel profile lines, the non-inclined curved interface and the bottom velocity model plane. The horizontal dimensions of the depicted part of the velocity model are 9.2 km x 3 km, the depth is 3 km. We compute and stack migrated sections in the 2-D plane located in the middle of the shot-receiver configuration, at horizontal coordinate x_2=5 km.

5. 3-D Kirchhoff prestack depth migration

We use the MODEL, CRT, FORMS and DATA packages for the Kirchhoff prestack depth migration (Červený, Klimeš & Pšenčík, 1988; Bulant, 1996). The migration consists of two-parametric ray tracing from the individual surface points, calculating grid values of travel times and amplitudes, performing the common-shot migration and stacking the migrated images. The shot-receiver configuration consists of 81 parallel profile lines at intervals of 0.025 km (see Figure 2). The first profile line is situated at horizontal coordinate $x_2 = 4$ km and the last profile line is situated at horizontal coordinate $x_2 = 6$ km.

For the purpose of our analysis, we calculate only one vertical image section corresponding to the central profile line ($x_2 = 5$ km, see Figure 2). Such an image represents one vertical section of full 3-D migrated volume. We form the image by computing and summing the corresponding contributions (images) from all 81 parallel source-receiver lines. While summing the contributions, the constructive interference focuses the migrated interface and the destructive interference reduces undesirable migration artifacts (non-specular reflections). We also use a cosine taper to clear some residua.

5.1 Migration using the correct velocity models with triclinic anisotropy and vertical gradients

We first migrate in the correct inhomogeneous single-layer velocity models with triclinic anisotropy and two different vertical gradients specified by matrices (1), (2) and (3) (TA-VG1 and TA-VG2 media), i.e. the anisotropy and vertical gradient in the velocity model for the migration is equal to the triclinic anisotropy and vertical gradient in the upper layer of the velocity model used to compute the recorded wave field. The migrated interface coincides nearly perfectly with the interface in the velocity model used to compute the recorded wave field. The migrated sections in Figure 3 demonstrate that the migration algorithm works well. These migrated sections may be used as a reference for comparison with the migrated sections calculated for inaccurate velocity models.

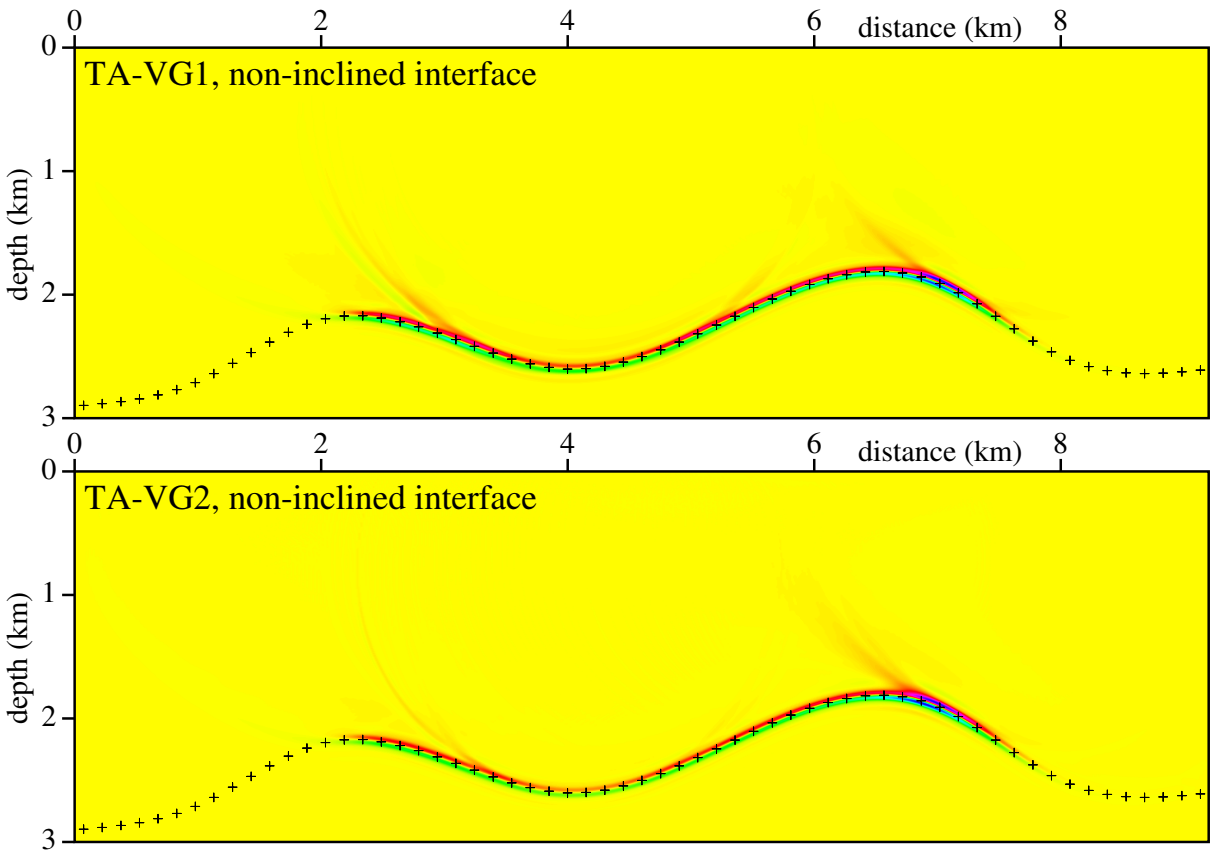

Figure 3. Stacked migrated sections calculated in the accurate velocity models without interfaces, specified by matrices (1), (2) and (3). The distribution of elastic moduli in the single-layer velocity models for migration is the same as the distribution in the upper layer of the velocity models used to calculate the recorded wave field. 81×240 common-shot prestack depth migrated sections, corresponding to 81 profile lines and 240 sources along each profile line, have been stacked. The crosses denote the interface in the velocity models used to compute the recorded wave field.

5.2. Migration using incorrect homogeneous velocity models

Now we use the Kirchhoff prestack depth migration to calculate migrated sections in incorrect homogeneous velocity models. These experiments simulate situations in which we have made an incorrect guess of the anisotropy and simple heterogeneity in the velocity model for migration.

a) Incorrect assumption of triclinic anisotropy without the gradient

The stacked migrated sections are calculated in incorrect homogeneous single-layer velocity models with triclinic anisotropy defined by matrices (5) and (6) (TA-VG1M and TA-VG2M media). Migrated interfaces coincide with original interfaces at the depth of $x_3 = 2.4125$ km (arithmetic mean of the depth of the curved interface). Parts of migrated interfaces positioned either deeper or less deeper than the arithmetic mean are analogously shifted vertically either upwards (undermigrated) or downwards (overmigrated), (see Figures 4a and 5a). The shift is larger if the velocity gradient is larger.

b) Incorrect assumption of VTI symmetry

In this case we migrate in incorrect homogeneous single-layer velocity models with a transversely isotropic medium with a vertical symmetry axis specified by matrices (7) and (8) (VTI-1-VG1M and VTI-1-VG2M media). Figures 4b and 5b show migrated interfaces. The segments of migrated interfaces in the horizontal range of approximately 4−8 km are defocused and distorted (caused by the combination of inaccurate anisotropy and vertical velocity gradients). In addition, note the poorly displayed migrated interface in the horizontal range of approximately 4−6 km (similar effect observed in Bucha (2011, 2012a) but not in Bucha (2012b)). The discussed segment of the interface (4−6 km) is worse for the model with the greater velocity gradient (matrix (8), VTI-1-VG2M medium) and the mispositioning of the migrated interface increases with the velocity gradient.

c) Incorrect assumption of HTI symmetry with the axis perpendicular to the profile lines

Here we migrate in incorrect homogeneous single-layer velocity models with a transversely isotropic medium with a horizontal symmetry axis defined by matrices (9) and (10) (HTI-2-VG1M and HTI-2-VG2M media). The segments of migrated interfaces in the horizontal ranges of approximately 2−4 km and 6−8 km are more defocused and distorted (see Figures 4c, 5c in comparison with Figures 4b, 5b). The migrated interface in the horizontal range of approximately 4−6 km is displayed much better in comparison with Section b. The mispositioning of the migrated interface increases with the velocity gradient.

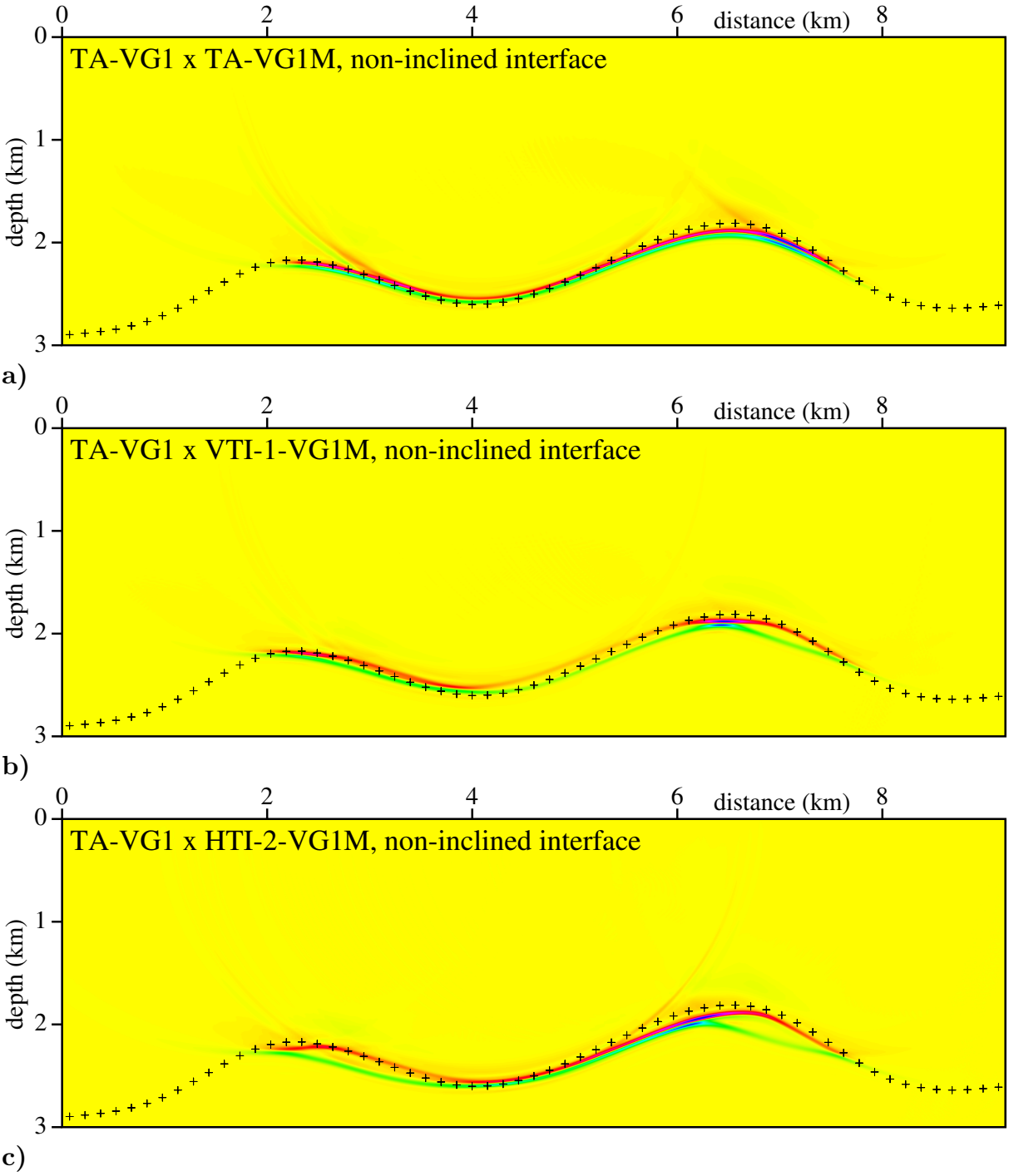

Figure 4. Images of the interface generated using incorrect homogeneous anisotropic velocity models specified by **a)** matrix (5), TA-VG1M medium, **b)** matrix (7), VTI-1-VG1M medium and **c)** matrix (9), HTI-2-VG1M medium. The anisotropy of the correct velocity model is triclinic and the gradient is vertical (matrices (1) and (3), TA-VG1 medium). 81×240 common-shot prestack depth migrated sections, corresponding to 81 profile lines and 240 sources along each profile line, have been stacked. The crosses denote the interface in the velocity model used to compute the recorded wave field.

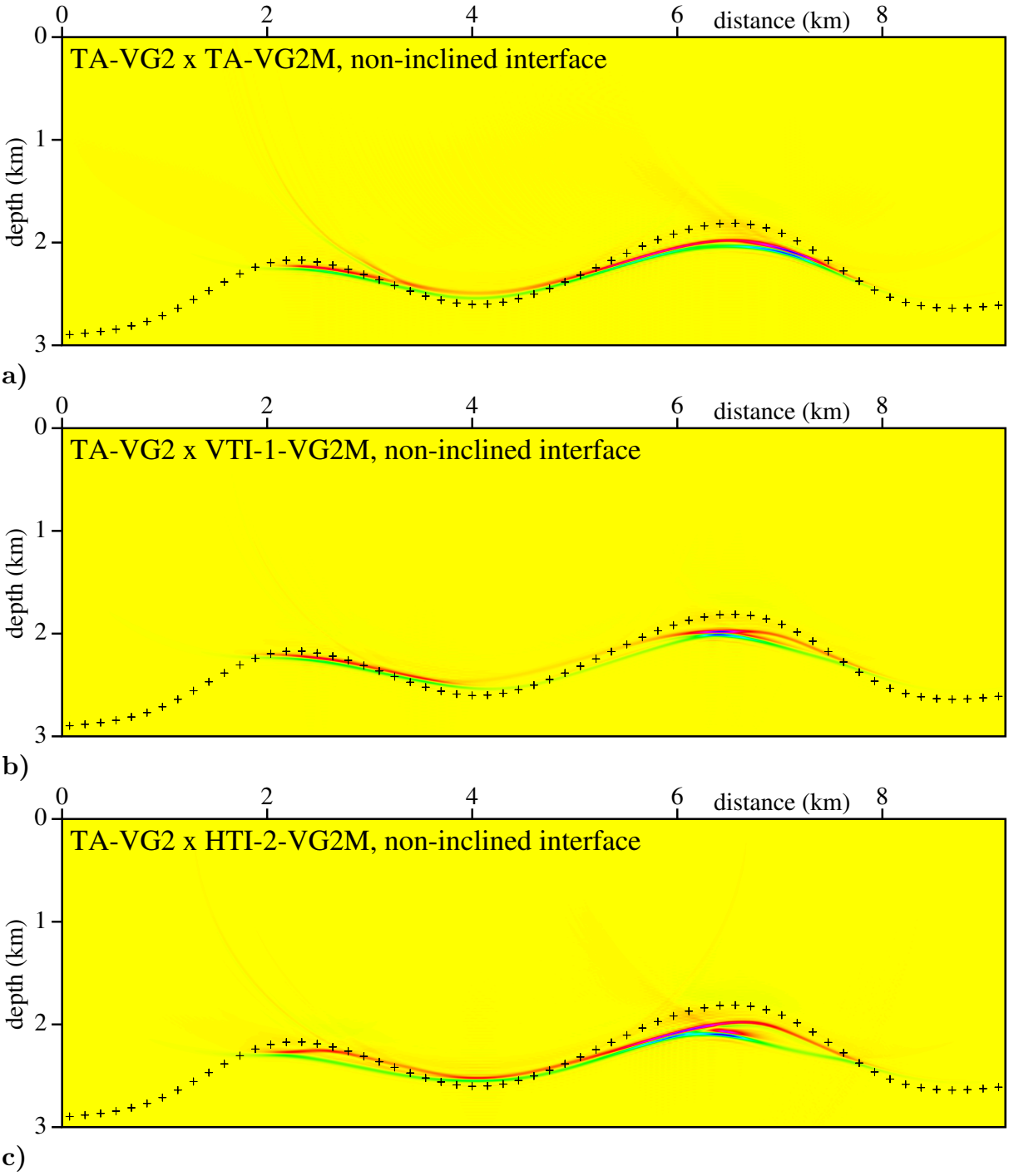

Figure 5. Images of the interface generated using incorrect homogeneous anisotropic velocity models specified by **a)** matrix (6), TA-VG2M medium, **b)** matrix (8), VTI-1-VG2M medium and **c)** matrix (10), HTI-2-VG2M medium. The anisotropy of the correct velocity model is triclinic and the gradient is vertical (matrices (2) and (3), TA-VG2 medium). 81×240 common-shot prestack depth migrated sections, corresponding to 81 profile lines and 240 sources along each profile line, have been stacked. The crosses denote the interface in the velocity model used to compute the recorded wave field.

The explanation of the poorly displayed parts of migrated interfaces is similar as in Bucha (2012a, 2012b). Figure 6 shows single common-shot images and explains the nearly vanishing inclined interface in the horizontal range of 4−6 km (see Figures 4b, 5b). Whereas the image migrated using the correct triclinic velocity model with the vertical gradient (matrices (2) and (3), TA-VG2 medium) is oriented correctly, the images migrated using the incorrect velocity model (matrix (8), VTI-1-VG2M medium) are rotated erroneously. When stacking the incorrect common-shot images, this rotation results in erasing the mentioned part of the interface due to destructive interference.

The poorly imaged interfaces in the horizontal ranges of 2−4 km and 6−8 km (see Figures 4c, 5c) are explained in Figures 7 and 8. The common-shot images migrated using the correct triclinic velocity model with the vertical gradient (matrices (2) and (3), TA-VG2 medium) look well, in contrast with the rotated and distorted images migrated using the incorrect velocity model (matrix (10), HTI-2-VG2M medium). While stacking the erroneous common-shot images, this rotation and distortion lead to defocusing and mispositioning of the mentioned part of the interface.

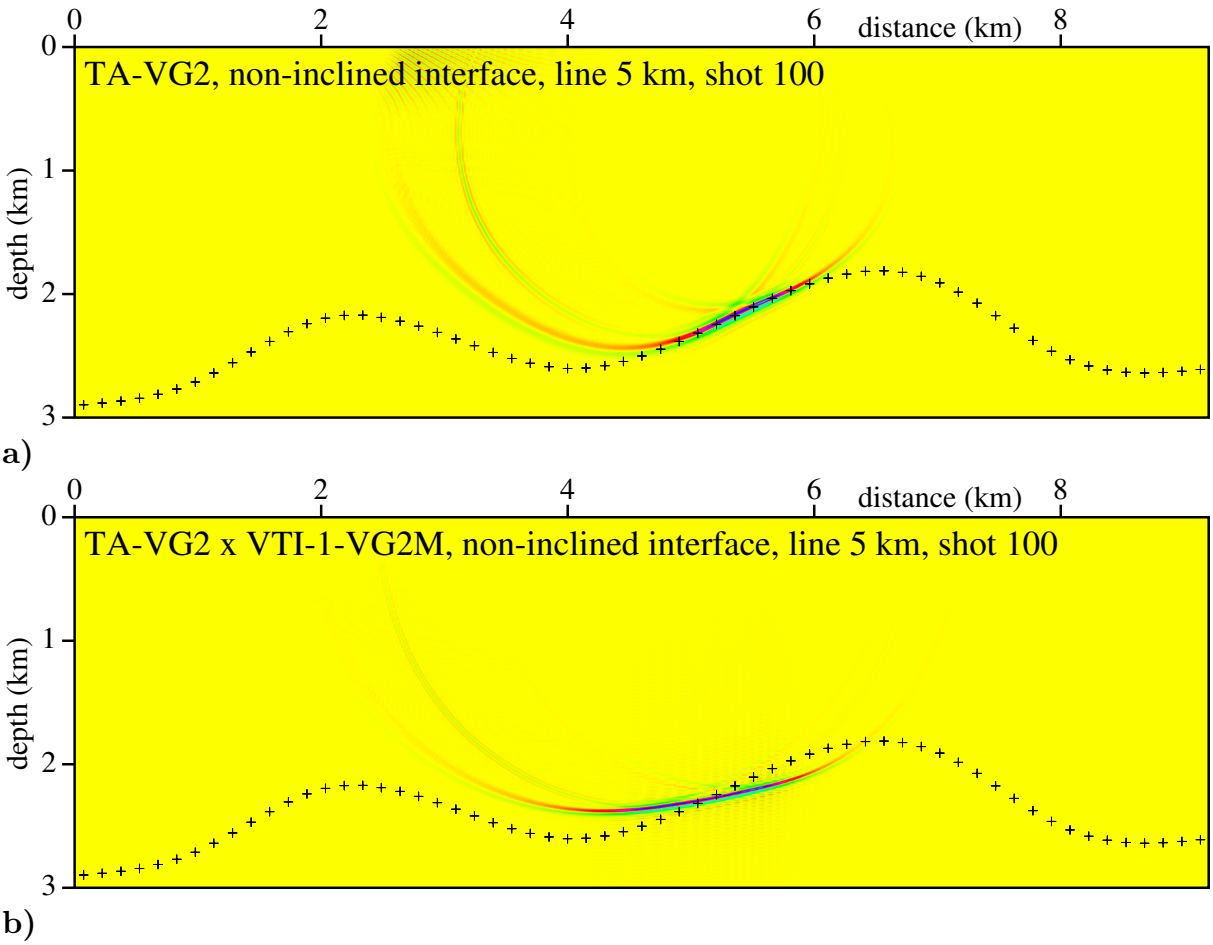

Figure 6. Prestack depth migrated images of the single common-shot gather at line $x_2 = 5$ km corresponding to shot 100 ($x_1 = 5.475$ km), migrated using **a)** the correct triclinic velocity model with the vertical gradient (matrices (2) and (3), TA-VG2 medium) and using **b)** the incorrect velocity model (matrix (8), VTI-1-VG2M medium). The crosses denote the interface in the velocity model used to compute the recorded wave field.

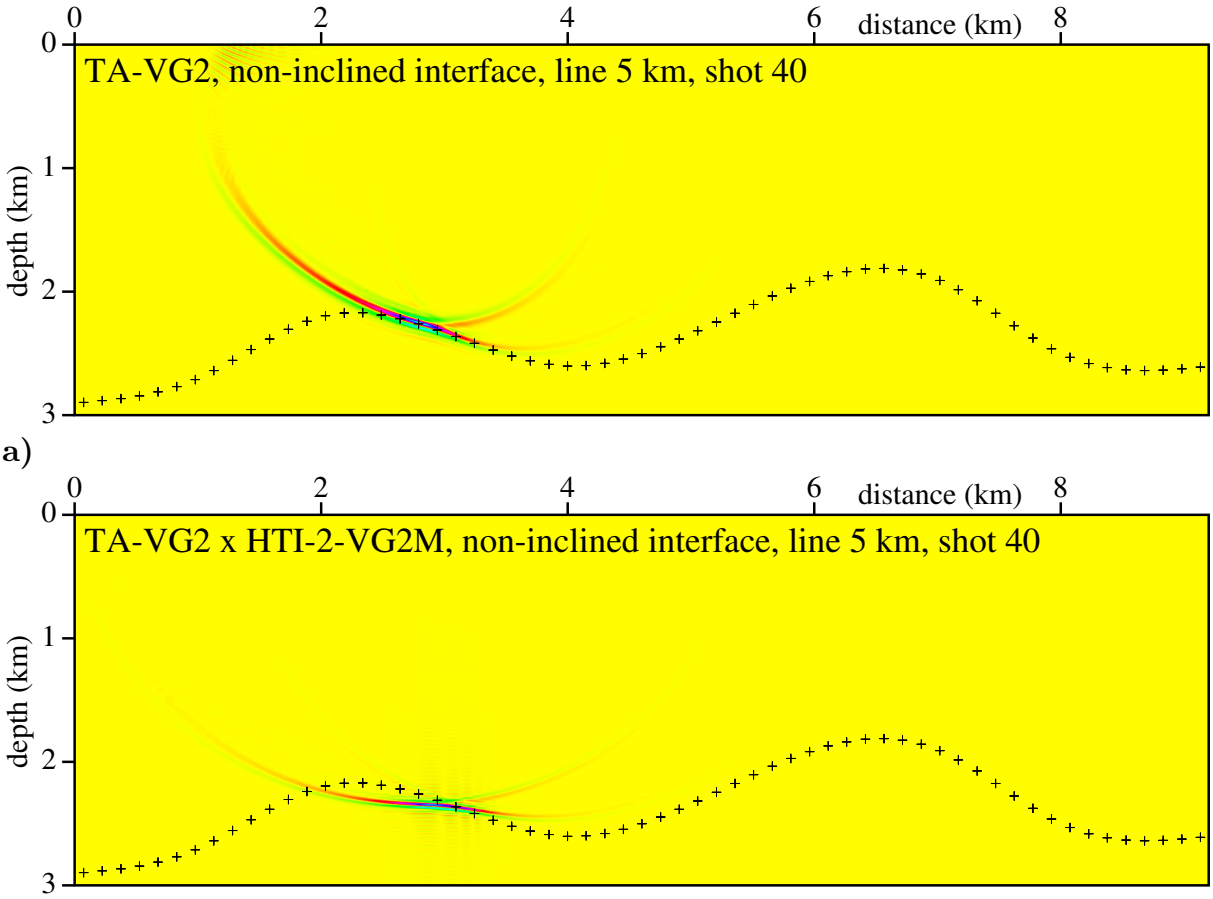

Figure 7. Prestack depth migrated images of the single common-shot gather at line $x_2 = 5$ km corresponding to shot 40 ($x_1 = 3.975$ km), migrated using **a)** the correct triclinic velocity model with the vertical gradient (matrices (2) and (3), TA-VG2 medium) and using **b)** the incorrect velocity model (matrix (10), HTI-2-VG2M medium). The crosses denote the interface in the velocity model used to compute the recorded wave field.

6. Conclusions

We have calculated synthetic data using an approximate ray theory in simple heterogeneous velocity models of relatively strong triclinic anisotropy and vertical velocity gradients. We have used the 3-D Kirchhoff prestack depth migration to generate migrated sections in heterogeneous and homogeneous velocity models

- with correct triclinic anisotropy and heterogeneity,
- with correct triclinic anisotropy and incorrect heterogeneity,
- with incorrect simpler anisotropies (VTI, HTI symmetries) and incorrect heterogeneity.

In the case of the correct triclinic anisotropy and heterogeneity (vertical velocity gradient), the migrated interface in the final stacked image coincides nearly perfectly with the interface in the model used to compute the recorded wave field.

In the case of the correct triclinic anisotropy and incorrect heterogeneity (model is homogeneous), the migrated interface coincides with the original interface at the depth where we have fitted elastic moduli. Other parts of the migrated interface are mispositioned (over or undermigrated). We did not observe significant distortion and defocusing.

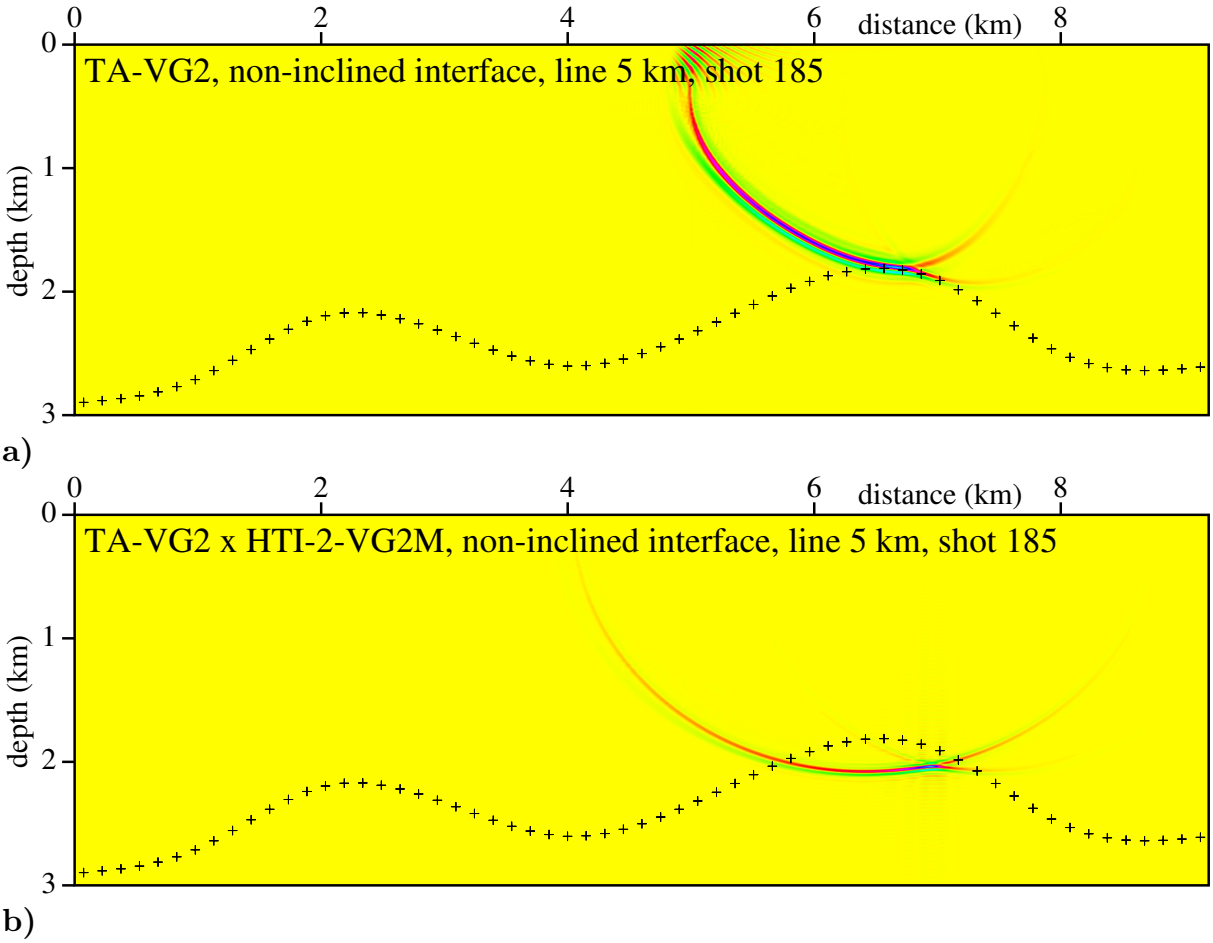

Figure 8. Prestack depth migrated images of the single common-shot gather at line $x_2 = 5$ km corresponding to shot 185 ($x_1 = 7.6$ km), migrated using **a)** the correct triclinic velocity model with the vertical gradient (matrices (2) and (3), TA-VG2 medium) and using **b)** the incorrect velocity model (matrix (10), HTI-2-VG2M medium). The crosses denote the interface in the velocity model used to compute the recorded wave field.

Finally, in the case of the incorrect simpler anisotropies (VTI, HTI symmetries) and incorrect heterogeneity (model is homogeneous), we observed mispositioning, distortion and defocusing of the migrated interface. The errors are caused by the combination of inaccurate anisotropy and inaccurate heterogeneity in the velocity models used for migration. Comparing selected migrated sections calculated in this paper and in Bucha (2012a), we can approximately separate the influence of the incorrect anisotropy and the incorrect heterogeneity. It is obvious, that the simple heterogeneity increases the errors of the migrated interface. We may expect the errors in migrated images of real structures, caused by the incorrect anisotropy and the incorrect heterogeneity, to be very difficult to distinguish.

Acknowledgments

The author thanks Luděk Klimeš and Ivan Pšenčík for help throughout the work on this paper.

The research has been supported by the Grant Agency of the Czech Republic under Contract P210/10/0736, by the Ministry of Education of the Czech Republic within Research Projects MSM0021620860 and CzechGeo/EPOS, and by the members of the consortium "Seismic Waves in Complex 3-D Structures" (see "http://sw3d.cz").

Appendix A: Averaging elastic moduli

We define elastic moduli with a vertical gradient:

$$A_{ij} = a_{ij} + b_{ij} z \quad , \tag{A1}$$

where

$$a_{ij} = A_{ij}(0) \quad ,$$

$$b_{ij} = \frac{A_{ij}(z_{max}) - A_{ij}(0)}{z_{max}} \quad ,$$

and z is the vertical coordinate (depth).

In our case, the squared vertical P-wave velocity (matrix element A_{33}) effects the result of migration most. It is better to average the slowness than the velocity or squared velocity. We thus average elastic moduli powered to $-\frac{1}{2}$ between depths $z = 0$ and $z = x_3$:

$$\begin{aligned}(A^0_{ij})^{-\frac{1}{2}} &= \frac{1}{x_3}\int_0^{x_3} \frac{1}{\sqrt{a_{ij} + b_{ij} z}} dz = \frac{1}{x_3}\frac{2}{b_{ij}}\left[\sqrt{a_{ij} + b_{ij} z}\right]_0^{x_3} \\ &= \frac{1}{x_3}\frac{2}{b_{ij}}(\sqrt{a_{ij} + b_{ij} x_3} - \sqrt{a_{ij}}) \quad .\end{aligned} \tag{A2}$$

The average reduced elastic moduli are then calculated according to:

$$\begin{aligned}A^0_{ij} = \left((A^0_{ij})^{-\frac{1}{2}}\right)^{-2} &= \frac{(b_{ij} x_3)^2}{4(\sqrt{a_{ij} + b_{ij} x_3} - \sqrt{a_{ij}})^2} = \frac{(b_{ij} x_3)^2(\sqrt{a_{ij} + b_{ij} x_3} + \sqrt{a_{ij}})^2}{4(b_{ij} x_3)^2} \\ &= \left(\frac{\sqrt{a_{ij} + b_{ij} x_3} + \sqrt{a_{ij}}}{2}\right)^2 = \left(\frac{\sqrt{A_{ij}(x_3)} + \sqrt{A_{ij}(0)}}{2}\right)^2 \quad .\end{aligned} \tag{A3}$$

References

Bulant, P. (1996): Two-point ray tracing in 3-D. *Pure appl. Geophys.*, **148**, 421-447.

Bucha, V. (2011): Kirchhoff prestack depth migration in 3-D models: Comparison of triclinic anisotropy with simpler anisotropies. In: *Seismic Waves in Complex 3-D Structures, Report 21*, pp. 47–62, Dep. Geophys., Charles Univ., Prague, online at "http://sw3d.cz".

Bucha, V. (2012a): Kirchhoff prestack depth migration in 3-D simple models: comparison of triclinic anisotropy with simpler anisotropies. *Stud. geophys. geod.*, **56**, 533–552.

Bucha, V. (2012b): Kirchhoff prestack depth migration in velocity models with and without gradients: Comparison of triclinic anisotropy with simpler anisotropies In: *Seismic Waves in Complex 3-D Structures, Report 22*, pp. 29–40, Dep. Geophys., Charles Univ., Prague, online at "http://sw3d.cz".

Červený, V., Klimeš, L. & Pšenčík, I. (1988): Complete seismic-ray tracing in three-dimensional structures. In: Doornbos, D.J. (ed.), *Seismological Algorithms*, Academic Press, New York, pp. 89–168.

Gajewski, D. & Pšenčík, I. (1990): Vertical seismic profile synthetics by dynamic ray tracing in laterally varying layered anisotropic structures. *J. geophys. Res.*, **95B**, 11301–11315.

Mensch, T. & Rasolofosaon, P. (1997): Elastic-wave velocities in anisotropic media of arbitrary symmetry-generalization of Thomsen's parameters ϵ, δ and γ. *Geophys. J. Int.*, **128**, 43–64.

Versteeg, R. J. & Grau, G. (eds.) (1991): *The Marmousi experience.* Proc. EAGE workshop on Practical Aspects of Seismic Data Inversion (Copenhagen, 1990), Eur. Assoc. Explor. Geophysicists, Zeist.